Research Square

Preprints are preliminary reports that have not undergone peer review.
They should not be considered conclusive, used to inform clinical practice,
or referenced by the media as validated information.

Integrative transcriptomic analysis and molecular dynamics simulations predict andrographolide - TLR3 interaction and potential anti-IAV immune responses

Yuan Wang
The Second Hospital of Nanjing, Affiliated to Nanjing University of Chinese Medicine
Zidu Xu
The Second Affiliated Hospital of Nanjing Medical University
Yang Chen
The Second Hospital of Nanjing, Affiliated to Nanjing University of Chinese Medicine
Yan Yang
The Second Hospital of Nanjing, Affiliated to Nanjing University of Chinese Medicine
Jingjing Guo
The Second Hospital of Nanjing, Affiliated to Nanjing University of Chinese Medicine
Yan Gu
guyan703@njucm.edu.cn

The Second Hospital of Nanjing, Affiliated to Nanjing University of Chinese Medicine

Research Article

Keywords: Andrographolide, Influenza A virus, TLR3, NK cell, Immunomodulation

Posted Date: November 24th, 2026

DOI: https://doi.org/10.21203/rs.3.rs-11722401/v1

License: This work is licensed under a Creative Commons Attribution 4.0 International License.
Read Full License

Additional Declarations: No competing interests reported.

Integrative transcriptomic analysis and molecular dynamics simulations predict andrographolide -TLR3 interaction and potential anti-IAV immune responses

Yuan Wang[2]*, Zidu Xu[3]*, Yang Chen[1], Yan Yang[1], Jingjing Guo[1#], Yan Gu[1#]

[1]Department of Geriatrics, The Second Hospital of Nanjing, Affiliated to Nanjing University of Chinese Medicine, Nanjing, PR China.

[2]Clinical Research Center, The Second Hospital of Nanjing, Affiliated to Nanjing University of Chinese Medicine, Nanjing, PR China.

[3]Department of Emergency, The Second Affiliated Hospital of Nanjing Medical University, Nanjing, PR, China.

*These authors have contributed equally to this work.

[#]Corresponding authors.

Email: guyan703@njucm.edu.cn

Abstract: Influenza A virus (IAV) remains a serious global public health threat. Andrographolide, the predominant bioactive component of Andrographis paniculata, exerts broad-spectrum antiviral effects. Nevertheless, the molecular targets and mechanisms underlying its anti-IAV activity remain unclear. This study intended to identify the key functional target of andrographolide and elucidate its immune regulatory mechanism against IAV infection. Bulk transcriptome sequencing, protein interaction network analysis and multiple machine learning methods were integrated to screen key functional genes regulated by andrographolide during IAV infection. Molecular docking and molecular dynamics simulations were used to verify the binding affinity between andrographolide and the hub gene, while single-cell transcriptomic analysis and virtual gene knockout assays were performed to explore cell-specific functional mechanisms. TLR3 was screened and confirmed as the core hub gene, and andrographolide could stably bind to TLR3. Single-cell results showed that TLR3 was specifically enriched in pulmonary NK cells of IAV-infected tissues; virtual TLR3 knockout significantly altered the transcriptional profiles of NK cells related to antiviral defense, cytotoxicity and cytokine signaling, confirming the critical regulatory function of TLR3. This transcriptomic analysis study verifies TLR3 as a direct functional target of andrographolide and identifies a novel NK cell-dependent immune axis, which provides a new mechanistic insight into the immunomodulatory and anti-influenza activity of andrographolide.

Keywords: Andrographolide; Influenza A virus; TLR3; NK cell; Immunomodulation.

1. Introduction

Influenza A virus (IAV) constitutes a prevalent pathogen responsible for human respiratory infection, triggering recurring seasonal outbreaks and occasional cross-species-derived pandemic threats[1]. The World Health Organization (WHO) reports that seasonal influenza causes an estimated 1 billion infections, 3-5 million severe cases, and 300000-500000 deaths annually worldwide[2]. Influenza A has imposed an enormous burden on healthcare systems and socioeconomic development, thus posing threat to global public health security[3].

Traditional Chinese medicine (TCM) has exhibited promising efficacy and favorable safety in the prophylaxis and treatment of influenza A[4]. Previous studies have illustrated that TCM exerts therapeutic effects on influenza A by exerting direct antiviral activity, mitigating pathological inflammation, regulating immune responses, and safeguarding organ function[5, 6]. Xiyanping (XYP), a proprietary Chinese medicinal preparation, has been clinically used for more than three decades to treat upper respiratory tract infections, viral pneumonia, influenza and bronchitis. Benefiting from its prominent antiviral and anti-inflammatory activities, XYP is extensively prescribed for diverse infectious respiratory disorders in clinical settings.[7, 8].

As the principal active component of Xiyanping, andrographolide is a natural diterpenoid compound endowed with a broad spectrum of bioactivities, such as anti-inflammatory, antibacterial, antineoplastic, cardioprotective, and immunomodulatory effects[9-11]. Notably, accumulating evidence has confirmed that andrographolide directly inhibits various influenza virus subtypes, yet the specific molecular mechanisms mediating its therapeutic effects against influenza A remain not fully understood[12-14].

This study integrated transcriptome sequencing, WGCNA and network pharmacology to predict anti-IAV targets of andrographolide, and screened TLR3 as the key hub gene via multiple machine learning models. Molecular docking was used to characterize the predicted interaction between andrographolide and TLR3, followed by molecular dynamics simulations to evaluate the dynamic stability of the predicted complex. Single-cell transcriptomics and in silico TLR3 perturbation analysis further revealed TLR3 enrichment in NK cells and predicted downstream immune pathway alterations, providing complementary computational evidence supporting a potential antiviral immunomodulatory mechanism of andrographolide and strengthening the robustness of our predictive findings.

2. Materials and methods

2.1 Collection of active ingredients and targets of andrographolide

Andrographolide was used as the search term to obtain its canonical SMILES string

and 2D structure from PubChem (https://pubchem.ncbi.nlm.nih.gov/). The canonical SMILES was imported into SwissTargetPrediction to predict potential molecular targets. Subsequently, relevant targets of andrographolide were retrieved from the CTD database (https://ctdbase.org/), GeneCards database (https://www.genecards.org/) and SuperPred database (https://prediction.charite.de/).

2.2 Gene expression analysis based on the GEO

The GSE206606 dataset was obtained from the Gene Expression Omnibus (GEO) database, comprising 12 IAV samples and 12 control samples. To identify differentially expressed genes (DEGs), we employed the "Limma" method by limma package in R (version 4.4.1)[15], based on a generalized linear model.

2.3 Weighted gene co-expression network analysis (WGCNA)

We applied Weighted Gene Co-Expression Network Analysis (WGCNA) to analyze gene correlations during IAV infection [16]. Genes with low variability were preliminarily filtered by median absolute deviation (MAD), with the least variable 50% excluded. DEG expression data was further refined to eliminate abnormal genes and samples, enabling the construction of a scale-free co-expression network. An optimal soft threshold (β) was adopted to compute gene adjacency, and the adjacency matrix was converted to a topological overlap matrix (TOM) for precise evaluation of gene connectivity. Gene modules were clustered via hierarchical clustering and dynamic tree cutting based on consistent gene expression patterns. Similar modules were merged according to the dissimilarity of module eigengenes. Venn analysis was finally used to intersect core module genes and DEGs, screening key genes closely related to IAV pathogenesis.

2.4 Construction of protein-protein interaction (PPI) networks

Potential targets related to influenza A and andrographolide were inputted into the STRING platform to construct a PPI network[17, 18]. Disconnected nodes were removed from the network, and an interaction score threshold of 0.400 was applied to retain medium-confidence and higher-confidence interactions. The resulting network data were imported into Cytoscape for visualization and biological network analysis. MCODE was utilized to identify tightly connected modules in the protein-protein

interaction network and quantify their topological characteristics. The nodes were color-coded to reflect their importance, with a higher score or index correlating with increased significance. Nodes of high importance were highlighted in red, indicating their potential key roles in the network. The drug-disease-target interaction network was subsequently visualized and constructed with Cytoscape 3.9.1.

2.5 GO enrichment analysis and KEGG pathway analysis

GO enrichment and KEGG pathway were analyzed by R package clusterProfiler. The biological processes (BP), molecular functions (MF), and cellular component (CC) of potential targets were screened to visualize and illustrate the relationships among compounds, targets, and pathways.

2.6 Single-gene gene set enrichment analysis (ssGSEA)

Single-gene ssGSEA was performed in R using GSVA, limma, and GSEABase packages to explore hub gene-related functional pathways during IAV infection[19]. Preprocessed expression data were grouped by the median hub gene expression. Standardized enrichment scores were calculated and normalized. Gene sets with $|NES| > 1$ and $P < 0.05$ were considered significantly enriched.

2.7 Identification of immune-infiltrating cells

Immune cell infiltration analysis was performed to characterize differences in the immune microenvironment between groups. The CIBERSORT algorithm was used to estimate the relative proportions of immune cell populations in control and IAV-infected samples from GSE206606. Differences in immune cell proportions between the two groups were assessed using the Wilcoxon rank-sum test and visualized using box plots.

2.8 Machine learning screening of characteristic genes

The R packages randomForest, glmnet and sigFeature were adopted to perform three machine learning approaches, namely random forest (RF), least absolute shrinkage and selection operator (LASSO) regression and support vector machine-recursive feature elimination (SVM-RFE), for screening characteristic genes among disease-related genes. Genes commonly identified by all three algorithms were obtained by calculating the intersection of screening results.

2.9 Molecular docking

The 2D chemical structure of andrographolide was collected in SDF format from PubChem and prepared using the LigPrep wizard in Schrdinger. The 3D structures was downloaded from PDB and prepared in Maestro 12.8 through preprocessing, refinement and minimization using the OPLS-2005 force field. The receptor binding site was defined using the Receptor Grid Generation module in Maestro. After ligand and receptor preparation, molecular docking was performed using the standard precision protocol of Glide. Docking scores were used to evaluate the predicted interactions, and ligand-protein interactions were visualized in PyMOL 2.5[20].

2.10 Molecular dynamics simulation

Molecular dynamics (MD) simulations were performed using GROMACS 2022[21]. The AMBER14SB force field was used for the receptor protein. Ligand topology and force-field parameters were generated using Sobtop 1.0 (dev3.1) with the GAFF2 force field, and ligand atomic charges were assigned using the RESP method. Structural and dynamic properties, including root-mean-square deviation (RMSD), root-mean-square fluctuation (RMSF), hydrogen bonds (HBonds), radius of gyration (Rg), and solvent-accessible surface area (SASA), were calculated using gmxrmsd, gmxrmsf, gmxhbond, gmxrgyr, and gmxsasa, respectively, to assess system stability, structural variation and solvent exposure.

2.11 Single-cell RNA-sequencing (scRNA-seq) analysis and Virtual knockout simulation analysis

ScRNA-seq data were obtained from the GEO under accession number GSE243629. The raw count matrix was processed using the R package Seurat (version 5.5.1). Harmony was applied for batch effect correction in PCA space to improve clustering accuracy. Clustree was used to construct clustering trees and determine the optimal clustering resolution. FeaturePlot function was used to visualize the expression of TLR3 on the t-SNE map. Differentially expressed genes between clusters were identified using the FindAllMarkers function.

Virtual knockout simulation: scTenifoldKnk was used to perform in silico perturbation of the target gene at the single-cell level and identify downstream genes predicted to be affected by the perturbation[22]. Genes with an adjusted $P < 0.05$ were

considered significantly differentially expressed. Functional enrichment analysis was performed on the resulting differentially expressed genes.

2.12 Statistic analysis

Statistical analyses were performed using GraphPad Prism (version 8.4.0) and R (version 4.4.1). Wilcoxon rank-sum test was used to assess the difference in the proportion of immune cells. Comparisons between the two groups were analyzed by t-test. *P*-values less than 0.05 were considered statistically significant.

3. Results

3.1. Identification of candidate genes in response to IAV infection

Using the Limma rapid differential analysis method, we identified a total of 2524 DEGs. Among them, 897 genes exhibited down-regulated expression, while 1627 genes were up-regulated. Volcano plots (Figure 1A) and heatmaps (Figure 1B) were created to visualize and analyze the expression patterns of these DEGs. SsGSEA revealed prominent enrichment of immune pathways such as the RIG-I-like receptor signaling pathway (Figure 1C). WGCNA grouped all genes into distinct co-expression modules (Figure 1D). Module-trait correlation analysis demonstrated that the green-yellow module exhibited the strongest positive correlation with IAV infection, defined as the core responsive module (Figure 1E). Venn analysis integrating DEGs and core module genes identified 678 overlapping candidates, which were selected for subsequent mechanistic investigation (Figure 1F).

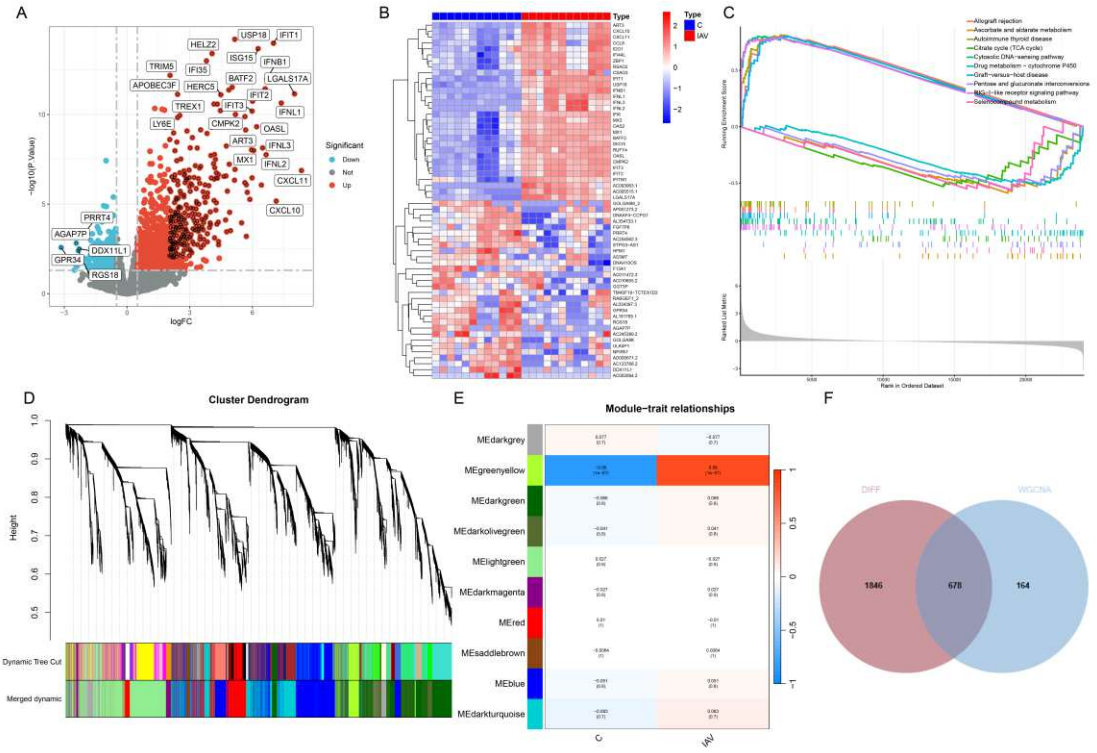


Figure 1 Transcriptomic profiling and WGCNA analysis upon IAV infection.(A) Volcano plot of DEGs. Red: upregulated genes; blue: downregulated genes; gray: non-significant genes. Representative genes are labeled. (B) Expression heatmap of top DEGs across samples. (C) GSEA enrichment curves of representative altered pathways. (D) WGCNA gene clustering dendrogram with dynamic tree-cut modules. (E) Module-trait correlation heatmap showing correlation coefficients and *P*-values. (F) Venn diagram showing overlaps between DEGs and WGCNA core module genes.

3.2 Identification of core targets of andrographolide against influenza A virus

Potential molecular targets of andrographolide were retrieved from SwissTargetPrediction, CTD, GeneCards and SuperPred databases. Duplicated records were subsequently excluded, resulting in 583 unique candidate targets. Venn analysis was performed by intersecting these targets with the aforementioned 678 selected key genes. A total of 16 overlapping genes were identified as candidate targets of andrographolide in IAV infection (Figure 2A). PPI networks revealed the interconnections among these candidate targets (Figure 2B, 2C), and six hub genes, namely STAT1, TLR3, PSMB9, IFITM1, IFI6 and TNFSF10, were further screened

according to degree values in the network. The compound-target-disease network visualized the relationships among andrographolide, candidate targets and influenza A virus (Figure 2D). Functional enrichment analysis revealed enrichment of virus-related biological processes, interferon responses and inflammasome activation (Figure 2E). KEGG pathway enrichment indicated that these intersecting genes were mainly involved in the Toll-like receptor signaling pathway, NOD-like receptor signaling pathway and necroptosis (Figure 2F). Figure 3 shows detailed enrichment results of intersecting genes in the influenza A signaling pathway. These signaling pathways are involved in host innate immunity against IAV. Notably, TLR3 serves as an important upstream mediator in the Toll-like receptor pathway[23], suggesting that TLR3 may represent a pharmacologically relevant candidate involved in the predicted anti-IAV effects of andrographolide. The figure helps clarify the potential functions of these genes and pathways in antiviral responses.

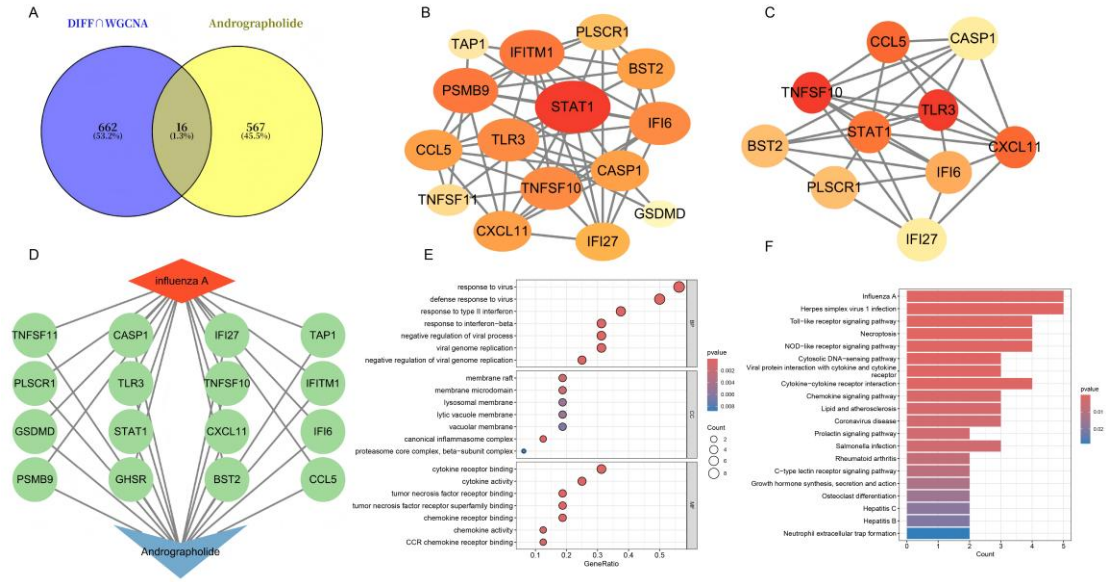


Figure 2 Screening and functional enrichment of core targets of andrographolide against IAV. (A) Venn diagram showing overlapping genes between andrographolide targets and DEGs-WGCNA candidate genes. (B, C) PPI network of core targets. Node color represents the connectivity degree. (D) Compound-target-influenza A virus interaction network. (E) Bubble diagram of GO enrichment analysis. (F) Bar plot of significantly enriched KEGG pathways.

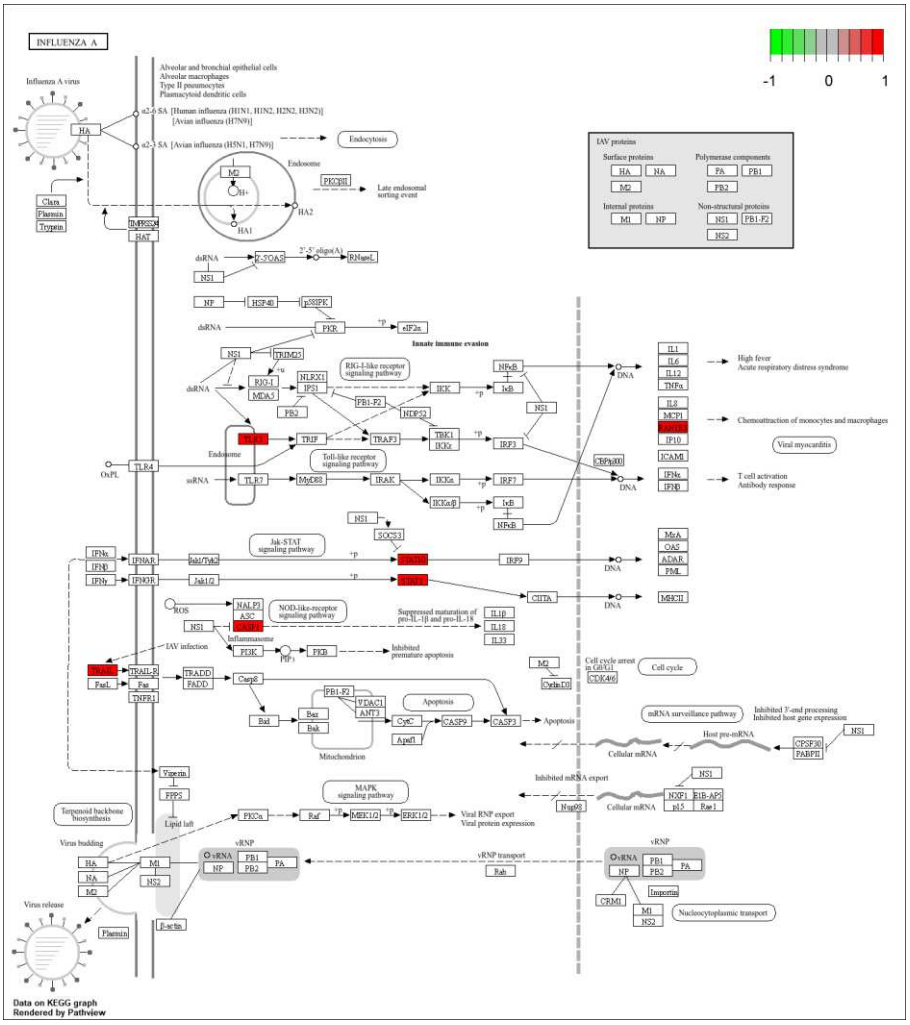


Figure 3 Influenza A signaling pathway in KEGG.

3.3 SsGSEA pathway analysis and analysis of immune infiltration results

To explore the biological pathways involving hub genes, we conducted ssGSEA on the six most significant hub genes. Consistent with previous enrichment results, these genes exhibited robust activation of multiple immune-related signaling pathways under IAV stimulation (Figure 4A). Therefore, the CIBERSORT algorithm was applied to quantify the proportion of infiltrated immune cells in control and IAV-infected samples. Significant differences in the infiltration levels of monocytes, M0 macrophages and M1 macrophages were observed between the two groups (Figure 4B-D). These results illustrated that IAV infection reshapes the immune microenvironment and suggested that the core genes may participate in anti-influenza responses via regulating myeloid immune cell infiltration.

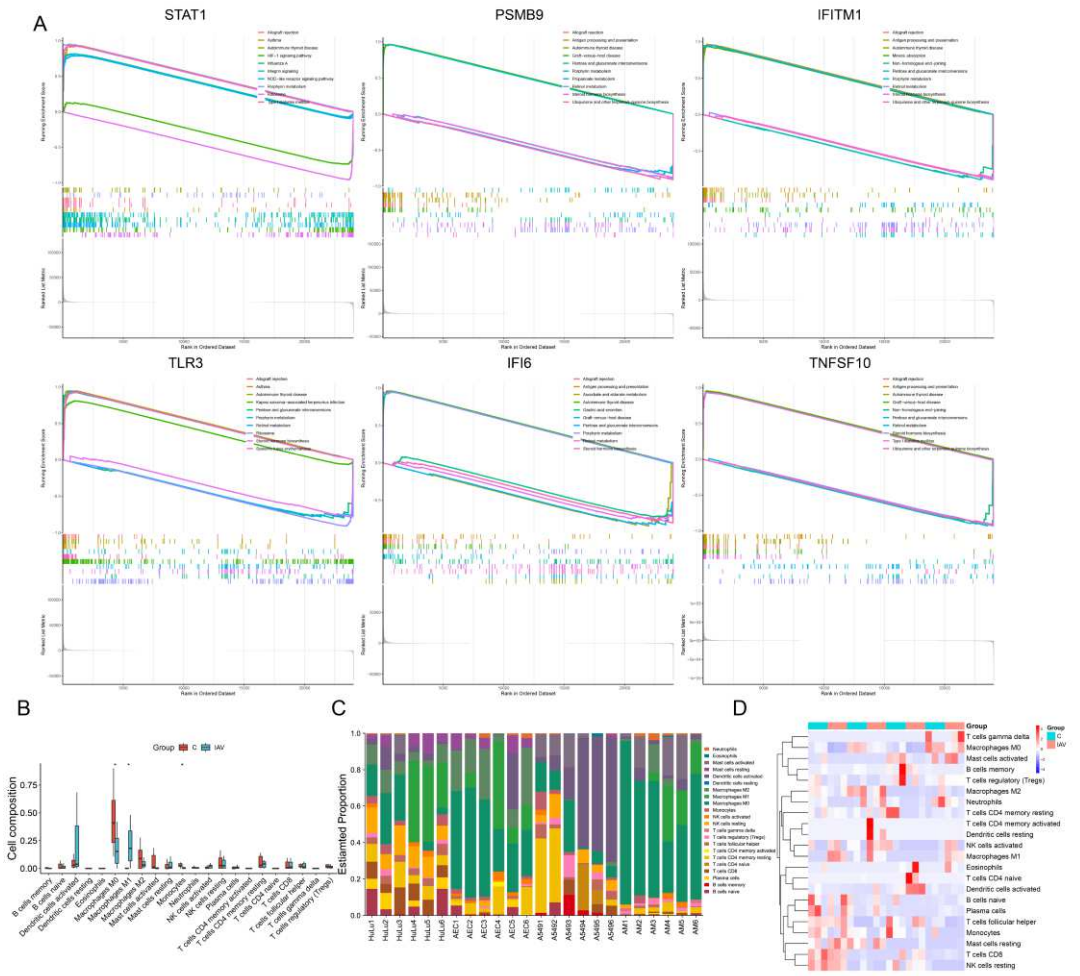


Figure 4 Pathway activity analysis of core genes and Immune infiltration. (A) SsGSEA plots showing enriched signaling pathways of representative core genes. (B) Box plot displaying differences in immune cell proportions between control and IAV groups. (C) Stacked bar chart presenting the immune cell fraction of each sample. (D) Heatmap showing correlation among different immune cell populations.

3.4 Identification of TLR3 as a Key Hub Gene Using Multiple Machine-Learning Algorithms

Three machine learning algorithms, LASSO regression, random forest (RF) and support vector machine (SVM), were applied to further screen candidate hub genes from the core targets. LASSO regression analysis identified feature genes by tuning the optimal lambda value (Figure 5A). The RF model was constructed, and gene importance ranking revealed that PSMB9, TLR3 and IFI27 exhibited the highest predictive importance (Figure 5B). Cross-validation was performed to determine the optimal feature number for each algorithm (Figure 5C). Subsequent Venn intersection

analysis identified TLR3 as the only overlapping gene shared by all three models, which was designated as the key hub gene closely associated with IAV infection (Figure 5D).

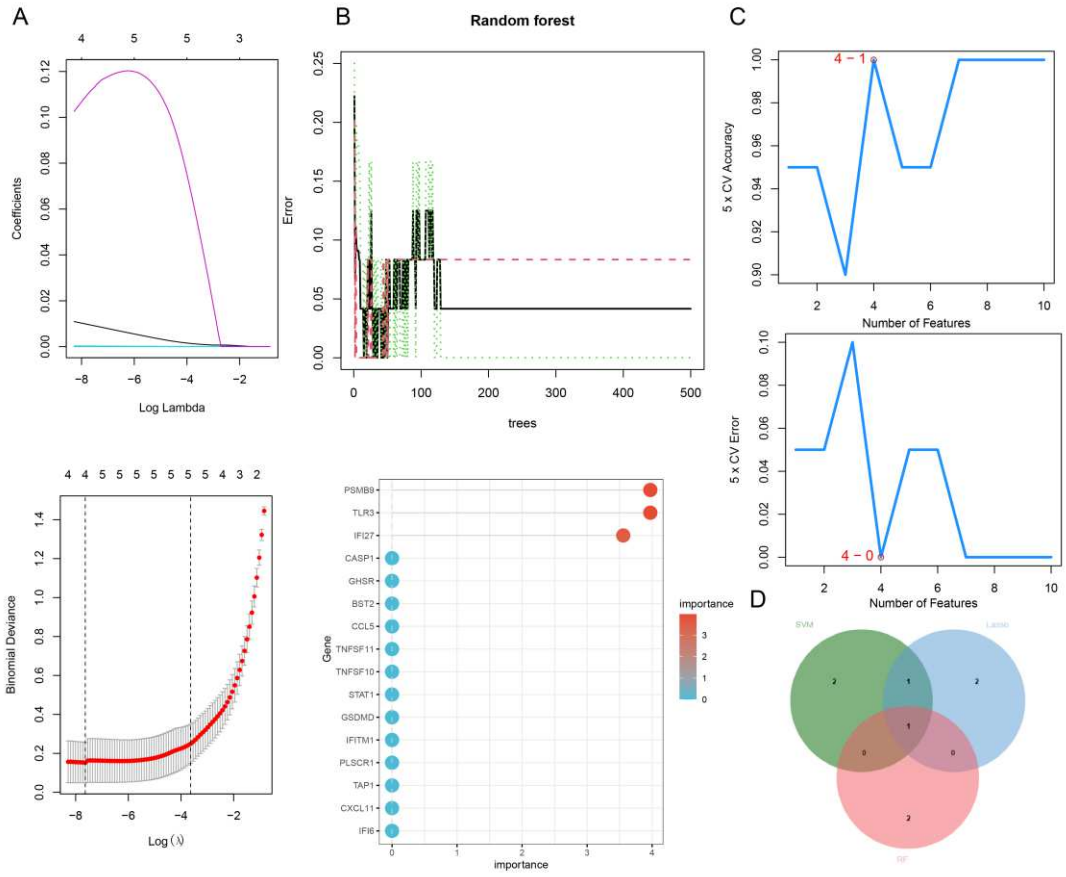


Figure 5 Machine learning-based screening of key hub genes. (A) Regression coefficient path diagrams for Lasso. (B) Error curve of RF model and gene importance ranking plot. (C) The SVM-RFE feature selection methods (D) Venn diagram showing overlapping genes obtained from LASSO, RF and SVM algorithms.

3.5 Results of Molecular docking and MD simulation

Based on the screening results, molecular docking was conducted between TLR3 and andrographolide. As illustrated in Figure 6A, andrographolide was predicted to occupy a binding pocket of TLR3, with a docking score of -5.0 kcal/mol and predicted interactions involving TYR207 and ASN285. A 100 ns all-atom MD simulation was performed to evaluate the dynamic stability of the predicted andrographolide-TLR3 complex. RMSD analysis (Figure 6B) showed that the complex reached equilibrium after approximately 20 ns and fluctuated around 0.18

nm, indicating that the predicted protein-ligand complex remained conformationally stable during the simulation. Radius of gyration (Rg) values (Figure 6C) exhibited minimal fluctuations, indicating limited global expansion or contraction and maintenance of structural compactness. SASA values showed relatively limited fluctuations throughout the simulation (Figure 6D), further supporting the structural stability of the predicted complex. Hydrogen-bond analysis (Figure 6E) revealed 0-3 intermolecular hydrogen bonds, with an average of approximately one, indicating persistent but variable hydrogen-bond interactions between andrographolide and TLR3 during the simulation. RMSF values of most TLR3 residues were <0.26 nm (Figure 6F), reflecting relatively limited residue flexibility in the simulated complex. The free energy landscape (FEL; Figure 6G), constructed with PC1 (Rg) and PC2 (RMSD), identified a low-free-energy basin at PC1 = 2.195 nm and PC2 = 0.14 nm, representing a relatively stable conformational state sampled during the simulation.

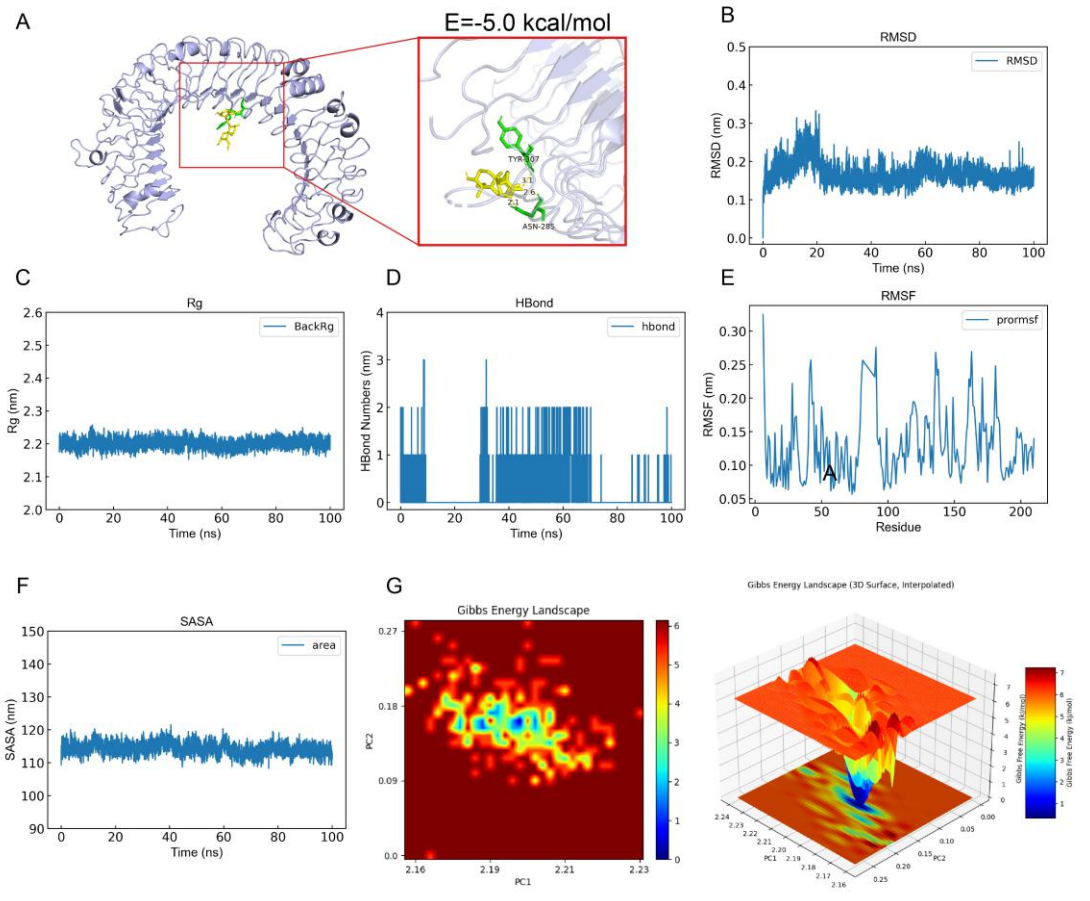


Figure 6 Molecular docking and molecular dynamics simulation analysis of

andrographolide bound to TLR3. (A) Molecular docking results of Andrographolide with TLR3. (B) RMSD values of the protein-ligand complex over simulation time. (C) Rg values of the protein-ligand complex over simulation time. (D) SASA values of the protein-ligand complex over simulation time. (E) Hydrogen bond (HBond) number of the protein-ligand complex over simulation time. (F) RMSF profile of the protein-ligand complex. (G) Free energy landscape.

3.6 scRNA-seq analysis and Virtual knockout simulation analysis

Single-cell RNA sequencing was applied to characterize the cellular distribution and transcriptional features of TLR3 within the immune microenvironment. t-SNE clustering partitioned all captured cells into nine immune cell subpopulations, including neutrophils, NK cells, $CD8^+$ T cells, monocytes, B cells and dendritic cells (Figure 7A). Feature plots illustrated the global expression pattern of TLR3 at single-cell resolution (Figure 7B). Violin dot plots further quantified the positive ratio and average expression level of TLR3 across individual immune subsets, indicating relatively high TLR3 expression in NK cells compared with other immune cell populations (Figure 7C). Predicted transcriptional alterations following in silico TLR3 perturbation were subsequently analyzed, and the top 20 genes with the most pronounced predicted expression changes are presented in Figure 7D. GO enrichment analysis highlighted alterations in biological processes associated with immune defense and cell-mediated cytotoxicity, alongside changes in granule components and receptor binding activity (Figure 7E). KEGG enrichment further indicated perturbation of signaling axes governing lymphocyte differentiation, phagocytosis and complement activation, which are relevant to host antiviral immunity. Taken together, single-cell profiling identified NK cells as a prominent cellular population expressing TLR3. In silico perturbation of TLR3 predicted extensive transcriptional remodeling of immune genes and alterations in multiple antiviral signaling circuits, suggesting that TLR3 may occupy an important regulatory position in NK-cell-associated antiviral responses during IAV infection.

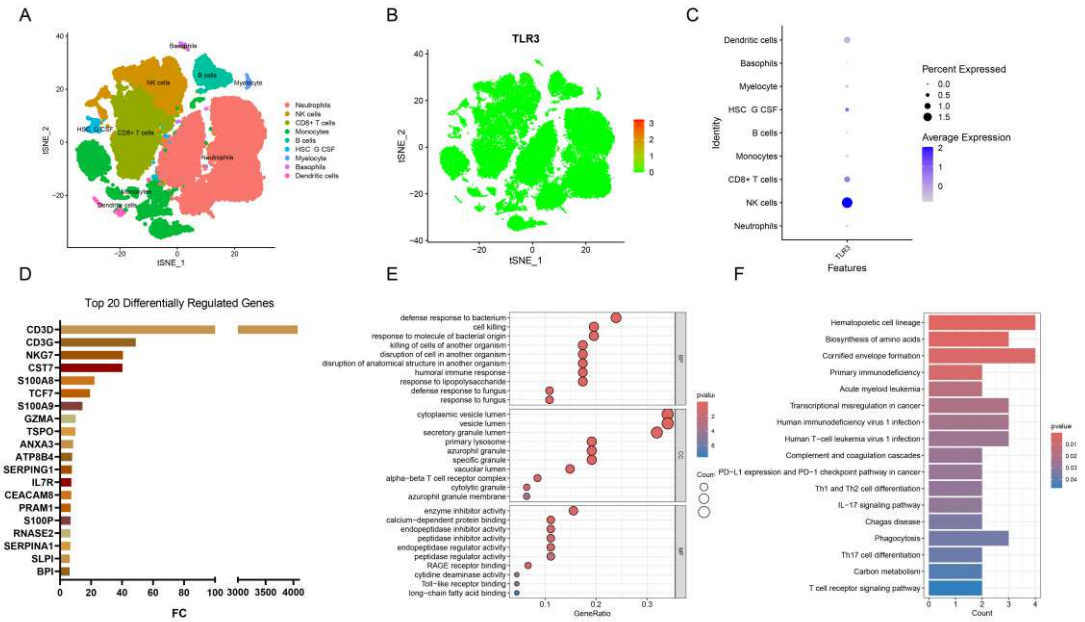


Figure 7 (A) t-SNE plot showing cell clusters colored by cell type ; (B) tSNE map displaying TLR3 expression in cells from 7A; (C) The bubble plot of 7B; (D) Virtual knockout experiment; (E) GO enrichment; (F) KEGG enrichment.

4. Discussion

In this study, we integrated transcriptomic analysis analyses, machine learning, molecular dynamics simulation and single-cell transcriptomics to investigate the potential anti-IAV mechanism and candidate targets of andrographolide. A total of 678 IAV-responsive key genes were screened via transcriptomic and WGCNA analyses, among which TLR3 was prioritized as a candidate antiviral hub gene through PPI network analysis and multiple machine-learning approaches. Molecular docking and molecular dynamics simulations supported a plausible and dynamically stable interaction between andrographolide and TLR3. Single-cell results further revealed TLR3 enrichment in NK cells, while in silico TLR3 perturbation predicted substantial remodeling of antiviral immune transcriptional programs, suggesting a potentially important regulatory role for TLR3 in NK-cell-associated antiviral immunity.

Conventionally, the antiviral function of TLR3 during IAV infection is thought to be mainly executed by epithelial cells and macrophages, where TLR3 activation initiates inflammatory signalling and mediates viral recognition[24, 25]. Most previous

mechanistic studies on andrographolide have focused on broad inflammatory suppression or global regulation of interferon pathways, but have not clearly defined a primary target cell population or cell-type-specific immune regulatory axis[13, 26, 27]. Notably, TLR3 expression in NK cells has been reported previously under certain conditions[28]; however, our data further indicate that, in the specific context of the IAV-infected lung microenvironment, NK cells represent a prominent cellular subset enriched in TLR3. This observation suggests that TLR3-dependent antiviral signaling may not be restricted to myeloid and epithelial cells and may also participate in NK-cell-associated immune surveillance. The predicted transcriptional changes following in silico TLR3 perturbation suggest that TLR3 may contribute to the maintenance of NK-cell antiviral transcriptional programs and downstream immune effector pathways. Unlike TLR3 signaling in dendritic cells[29, 30], which primarily bridges innate and adaptive immunity, TLR3 expression in NK cells may enable integration of pathogen-sensing signals with downstream antiviral effector responses before adaptive immunity is fully established[31]. Collectively, our findings support a previously underappreciated TLR3-associated antiviral regulatory axis in NK cells and suggest a potential link between andrographolide, host innate immune signaling and antiviral responses. This cell-specific hypothesis extends the current understanding of how andrographolide may influence IAV-associated immunity and provides a direction for investigating the immunomodulatory effects of natural compounds through pattern-recognition receptor signaling in NK cells. From a translational perspective, modulation of the TLR3-associated NK-cell response may represent a potential host-directed strategy for further investigation in influenza. Such a host-directed mechanism could theoretically complement direct-acting antiviral strategies, although this possibility requires experimental and clinical validation.

Despite the above findings, several limitations of this study should be acknowledged. First, the major conclusions are based on integrative computational analyses, public transcriptomic datasets, molecular docking and molecular dynamics simulations. Therefore, the predicted regulatory relationship among andrographolide, TLR3 and NK-cell antiviral responses requires direct validation using biochemical binding

assays, cell-based experiments and appropriate in vivo models. Second, this study mainly focused on andrographolide alone, while the synergistic antiviral effects of multiple active ingredients derived from Xiyanping were not considered. Subsequent multi-component analyses may help clarify the broader pharmacological mechanism of the preparation.

In conclusion, this study identifies TLR3 as a potential pharmacological target associated with the anti-IAV activity of andrographolide and highlights a possible NK-cell-centered immune regulatory context. By integrating bulk transcriptomics, machine learning, molecular simulation, single-cell transcriptomics and in silico gene perturbation, our findings provide multilayer computational evidence supporting a potential andrographolide–TLR3–NK-cell axis during IAV infection. Further biochemical, cellular and in vivo studies are required to validate this proposed mechanism and determine its pharmacological relevance.

Conflicts of interest: Authors declare no conflicts of interest.

Funding： This study was supported by Nanjing Second Hospital Talent Promotion Project (No. RCZD24005); Nanjing Infectious Disease Clinical Medical Center; Innovation Center for Infectious Disease of Jiangsu Province (NO. CXZX202232), Nanjing, PR, China.

Data availability: The datasets used and analyzed during thecurrent study are available from the corresponding author onreasonable request.

Trial registration： Not applicable.

Ethics, Consent to Participate, and Consent to Publish declarations: not applicable.

References

[1] DEL RICCIO M, CAINI S. Global influenza epidemiology after 2020: patterns of circulation, epidemic timing and duration, and implications for vaccination strategies [J]. Euro surveillance : bulletin Europeen sur les maladies transmissibles = European communicable disease bulletin, 2026, 31(21).

[2] KRAMMER F, SMITH G J D, FOUCHIER R A M, et al. Influenza [J]. Nature Reviews Disease Primers, 2018, 4(1): 3.

[3] SPINARDI J R, THAKKAR K B, WELCH V L, et al. The need for novel influenza vaccines in low- and middle-income countries: A narrative review [J]. The Brazilian journal of infectious diseases : an official publication of the Brazilian Society of Infectious Diseases, 2025, 29(1): 104465.

[4] HE F, XU J, YU T, et al. Traditional Chinese medicine in influenza treatment: a bibliometric analysis integrating multiple databases [J]. Frontiers in microbiology, 2026, 17: 1761339.

[5] LIU M, HAN S, SHI N, et al. Research progress in the inhibitory mechanisms of traditional Chinese medicine therapies against influenza A [J]. Frontiers in immunology, 2026, 17: 1764099.

[6] XIONG Y, LI N X, DUAN N, et al. Traditional Chinese Medicine in Treating Influenza: From Basic Science to Clinical Applications [J]. Frontiers in pharmacology, 2020, 11: 575803.

[7] LIU X, LIU B, WANG S, et al. Research Progress on Traditional Chinese Medicine Preparations in Respiratory Inflammatory Diseases [J]. Journal of inflammation research, 2026, 19: 545874.

[8] ZHANG X Y, LV L, ZHOU Y L, et al. Efficacy and safety of Xiyanping injection in the treatment of COVID-19: A multicenter, prospective, open-label and randomized controlled trial [J]. Phytother Res, 2021, 35(8): 4401-10.

[9] LI X, YUAN W, WU J, et al. Andrographolide, a natural anti-inflammatory agent: An Update [J]. Frontiers in pharmacology, 2022, 13: 920435.

[10] GONDE D P, BHOLE B K, KAKAD K S. Andrographolide, diterpenoid constituent of Andrographis paniculata: Review on botany, phytochemistry, molecular docking analysis, and pharmacology [J]. Annales Pharmaceutiques Françaises, 2024, 82(1): 15-43.

[11] ZHANG H, LI S, SI Y, et al. Andrographolide and its derivatives: Current achievements and future perspectives [J]. European journal of medicinal chemistry, 2021, 224: 113710.

[12] ADIGUNA S P, PANGGABEAN J A, ATIKANA A, et al. Antiviral Activities of Andrographolide and Its Derivatives: Mechanism of Action and Delivery System [J]. Pharmaceuticals (Basel), 2021, 14(11).

[13] YANG W, HE Q, SUN Z, et al. Andrographolide Suppresses Influenza A Virus-Induced Pyroptosis via PI3K/AKT-Mediated Caspase-3/GSDME Inactivation [J]. Biomedicines, 2026, 14(4).

[14] LI X, YUAN W, WU J, et al. Andrographolide, a natural anti-inflammatory agent: An Update [J]. Frontiers in pharmacology, 2022, Volume 13 - 2022.

[15] RITCHIE M E, PHIPSON B, WU D, et al. limma powers differential expression analyses for RNA-sequencing and microarray studies [J]. Nucleic acids research, 2015, 43(7): e47.

[16] LANGFELDER P, HORVATH S. WGCNA: an R package for weighted correlation network analysis [J]. BMC Bioinformatics, 2008, 9(1): 559.

[17] SHANNON P, MARKIEL A, OZIER O, et al. Cytoscape: A Software Environment for Integrated Models of Biomolecular Interaction Networks [J]. Genome Research, 13(11): 2498-504.

[18] SZKLARCZYK D, GABLE A L, NASTOU K C, et al. The STRING database in 2021: customizable protein-protein networks, and functional characterization of user-uploaded gene/measurement sets [J]. Nucleic acids research, 2021, 49(D1): D605-d12.

[19] CANZLER S, HACKERMüLLER J. multiGSEA: a GSEA-based pathway enrichment analysis for transcriptomic analysis data [J]. BMC Bioinformatics, 2020, 21(1): 561.

[20] MORRIS G M, HUEY R, LINDSTROM W, et al. AutoDock4 and AutoDockTools4: Automated docking with selective receptor flexibility [J]. Journal of computational chemistry, 2009, 30(16): 2785-91.

[21] RAKHSHANI H, DEHGHANIAN E, RAHATI A. Enhanced GROMACS: toward a better numerical simulation framework [J]. Journal of molecular modeling, 2019, 25(12): 355.

[22] OSORIO D, ZHONG Y, LI G, et al. scTenifoldKnk: An efficient virtual knockout tool for gene function predictions via single-cell gene regulatory network perturbation [J]. Patterns (New York, NY), 2022, 3(3): 100434.

[23] DUAN T, DU Y, XING C, et al. Toll-Like Receptor Signaling and Its Role in Cell-Mediated Immunity [J]. Frontiers in immunology, 2022, 13: 812774.

[24] KAYESH M E H, KOHARA M, TSUKIYAMA-KOHARA K. Recent Insights into the Molecular Mechanisms of the Toll-like Receptor Response to Influenza Virus Infection [J]. International journal of molecular sciences, 2024, 25(11): 5909.

[25] LI H, WANG A, ZHANG Y, et al. Diverse roles of lung macrophages in the immune response to influenza A virus [J]. Frontiers in microbiology, 2023, 14: 1260543.

[26] YANG W, HE Q, SUN Z, et al. Andrographolide Suppresses Influenza A Virus-Induced Pyroptosis via PI3K/AKT-Mediated Caspase-3/GSDME Inactivation [J]. Biomedicines, 2026, 14(4): 887.

[27] CUI Y, YUE Y, LIN H, et al. Combination of andrographolide and baicalin inhibited influenza A virus infection through suppressing RORγt-IL-17A pathway [J]. Phytomedicine : international journal of phytotherapy and phytopharmacology, 2026, 156: 158277.

[28] SIVORI S, FALCO M, CARLOMAGNO S, et al. Heterogeneity of TLR3 mRNA transcripts and responsiveness to poly (I:C) in human NK cells derived from different donors [J]. International immunology, 2007, 19(12): 1341-8.

[29] MATSUMOTO M, TAKEDA Y, TATEMATSU M, et al. Toll-Like Receptor 3 Signal in Dendritic Cells Benefits Cancer Immunotherapy [J]. Frontiers in immunology, 2017, 8: 1897.

[30] FRANK K, PAUST S. Dynamic Natural Killer Cell and T Cell Responses to Influenza Infection [J]. Frontiers in cellular and infection microbiology, 2020, Volume 10 - 2020.

[31] HSIEH M L, NISHIZAKI D, ADASHEK J J, et al. Toll-like receptor 3: a double-edged sword [J]. Biomarker Research, 2025, 13(1): 32.